

**Haris Moazam Sheikh<sup>1</sup>**

Department of Mechanical Engineering,  
University of California, Berkeley,  
Berkeley, CA 94720, USA  
email: harissheikh@berkeley.edu

**Sangjoon Lee**

Department of Mechanical Engineering,  
University of California, Berkeley,  
Berkeley, CA 94720, USA  
email: sangjoonlee@berkeley.edu

**Jinge Wang**

Department of Mechanical Engineering,  
University of California, Berkeley,  
Berkeley, CA 94720, USA  
email: jinge@berkeley.edu

**Philip S. Marcus**

Department of Mechanical Engineering,  
University of California, Berkeley,  
Berkeley, CA 94720 USA  
email: pmarcus@me.berkeley.edu

# Airfoil Optimization using Design-by-Morphing

*We present Design-by-Morphing (DbM), a novel design methodology applicable to creating a search space for topology optimization of 2D airfoils. Most design techniques impose geometric constraints and sometimes designers' bias on the design space itself, thus restricting the novelty of the designs created, and only allowing for small local changes. We show that DbM methodology does not impose any such restrictions on the design space and allows for extrapolation from the search space, thus granting truly radical and large search space with a few design parameters. In comparison to other shape design methodologies, we apply DbM to create a search space for 2D airfoils. We optimize this airfoil shape design space for maximizing the lift-over-drag ratio,  $CLD_{max}$ , and stall angle tolerance,  $\Delta\alpha$ . Using a bi-objective genetic algorithm to optimize the DbM space, it is found that we create a Pareto-front of radical airfoils exhibiting remarkable properties for both objectives.*

**Keywords:** Design-by-Morphing (DbM), Topology Optimization, Airfoils

## 1 Introduction

Optimizing the shape of an airfoil is an integral design stage for aerodynamic components like aircraft wings[1–4] and wind-turbine blades[5–10]. A typical airfoil optimization process contains three main components: shape parameterization, airfoil evaluation, and optimization, among which the parameterization method determines both the design space and the complexity of the optimization problem. Hence, a desirable parameterization technique is required to cover an extensive design space within a limited number of design parameters[11–14], which is especially significant during the early design stage when minimum geometric constraints are placed as well as when radical changes during the optimization process are welcomed.

Different shape parameterization methods offer different fidelity and ranges of control[11,13,15]. According to the scope of the design parameters, one can place these methods on a spectrum where, on one end, the change of one parameter affects only a local section of the airfoil shape thus offering delicate control of the shape, and, on the other end, each design parameter affects the airfoil's global contour[11].

On the local end of the spectrum is the discrete method[16], whose design parameters are exactly the discrete surface points that define the airfoil shapes. Since the displacement of each point can be adjusted, the design space is potentially limitless[17] and very fine local control with high fidelity can be achieved. However, a large number of surface points are needed in general to describe an airfoil shape accurately, which increases the complexity of the optimization problem. As a result, one usually relies on gradient-based method to guide the optimization which is limited to small local changes that can easily get stuck at a local optimum.

Increasing the geometrical extent of each parameter's influence, one would find classical methods that determine the airfoil shape based on the regional features or the control points and perform curve-fittings of some kind. For example, the popular parametric section (PARSEC) method[18] uses eleven (or twelve) parameters that represent major sectional features of an airfoil, in-

cluding leading edge radii and upper and lower crest locations, and approximate the airfoil surface using a 6<sup>th</sup> order polynomial. Another popular method would be the Bézier parameterization[19], which forms the upper and the lower surfaces of the airfoil through the Bézier curves defined by the control points chosen in advance. Additionally, a combination of the two techniques, Bézier-PARSEC parameterization[20], also exists, which creates Bézier curves using the parameters of the PARSEC method and combines these curves to form the shape contours. One main issue with the above methods is their inability or inefficiency to include high-fidelity features: the PARSEC and the Bézier-PARSEC method both have fixed number of parameters and offer very limited range of fidelity, while the Bézier parameterization requires higher-degree Bézier curves to describe complex shapes, which become inefficient to calculate as the order increases[17].

To take into consideration high-fidelity features of airfoils or, equivalently, represent more complex curves, either B-splines[21, 22] or nonuniform rational B-spline (NURBS)[23] may be considered. These methods form curves by connecting low-order Bézier segments defined by the control points. With denser control points, these methods naturally move to the local end of the spectrum capable of representing high-fidelity features whereas computing complexity increases at the same time as a expense. In an effort to reduce the number of the design parameters, the control points may be grouped together, and global transformations such as twisting and thickening can be used as the parameters instead. It is known as the free-form deformation (FFD) method[24,25] and is closer to the global end of the spectrum. A similar method, which is called radial basis function domain element (RBF) approach[26–28], also exists and makes use of radial basis function to exert deformation on the airfoil.

Paying more attention to the global end of the spectrum, we see other methods that use spectral construction of basis functions or modes to form or deform airfoil shapes. One typical way of determining the bases is using the orthogonal modes obtained via singular value decomposition (SVD) of a given large set of airfoil data, where the dimensionality can be reduced by using only first few dominant modes[29–33]. Other methods include the Hicks-Henne approach[34],

<sup>1</sup>Corresponding Author.

Version 1.18, December 19, 2022

which uses a linear combination of sinusoidal functions to create ‘bumps’ on the airfoil surface in a deformative manner, and class/shape function transformation (CST) method proposed by Kulfan[35,36], which represents an airfoil shape as the product of a class function and a shape function generated by a linear combination of Bernstein polynomials. However, like most of the other methods on the spectrum, they require more number of basis functions/modes in order to resemble high-fidelity features, which again falls into the so-called the *curse of dimensionality*.

There have been attempts that aim to reduce the number of parameters needed while capturing a large enough design space[37–39]. A recent one, for instance, was conducted by Chen et al.[40], who used a deep generative model, called B  zier-GAN, to parameterize airfoil shapes by learning from the major shape variations in an existing database. Furthermore, they preserve the minor features of the airfoil shapes via a noise space, which allows them to separate the major and the minor features hence leading to a faster design space exploration. However, this study, like many other dimension reduction methods, relies on the assumption that the optimum design is not far from an existing database, which is not always true. Chen and Ahmed recently proposed a new GAN-based method[41] that aimed to overcome this limitation by encouraging diversity during sample generations. On the other hand, we mainly consider the shape parameterization technique for the early design stage and prefer not to make the same assumption. In particular, we are interested in a method that would contain high-order features while keeping a limited number of design parameters and allowing radical change from the initial airfoil shapes.

In this paper, we apply the Design-by-Morphing (DbM) parameterization technique to the airfoil optimization problem. DbM is a novel, universal design strategy that was first introduced by Oh et al.[42] and that has been used in recent years for geometry optimization of different problems[42–45]. Specifically, the DbM method ‘morphs’ homeomorphic baseline shapes together to create new shapes and can extrapolate as well as interpolate the design space, which allows for both the high-fidelity representation of shapes without the curse of dimensionality and radical improvements in the shapes without any implicit geometric constraints[42,44]. On the spectrum of methods mentioned above, DbM can be posited in the global end of the spectrum. The strategy is expectedly applicable to a variety of both 2D and 3D design problems and we aim at conducting a special case study of DbM for the 2D airfoil shape optimization here. Throughout this paper, we expect to make the following scientific contributions:

- Application of DbM to 2D airfoil shape optimization, allowing for both accurate reconstruction of the existing airfoil database and radical change of airfoil shapes while being free from geometric constraints and designers’ biases.
- Evaluation of representation capacity of DbM strategy and comparison of DbM with other typical 2D airfoil design strategies.
- Optimization of the search space created by DbM of 2D airfoils using a genetic algorithm and investigation of the optimum Pareto-front.

## 2 Design-by-Morphing

Design-by-Morphing (DbM) works by morphing homeomorphic, i.e. topologically equivalent, shapes to create a continuous and constraint-free design search space that can produce radical extrapolated shapes, which is a unique feature compared to other existing design strategies. Furthermore, DbM is extendable to any physical dimensions (2D or 3D) and applicable to a wide range of design problems [42,44]. The details of DbM are presented in the subsequent subsections.

**2.1 Baseline Shapes and Morphing.** The DbM technique generally requires two or more homeomorphic ‘baseline shapes’,

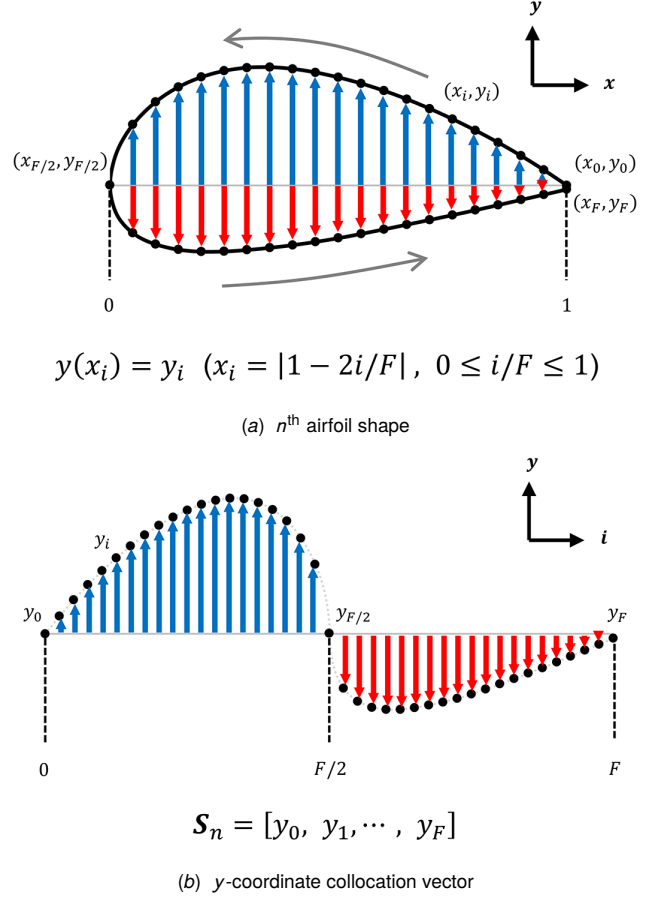


**Fig. 1 An example of DbM. The coordinates of the baseline shapes are weighted, summed, and normalized to form the coordinates of a morphed shape.**

mostly chosen from pre-existing designs in the literature, for the design search space creation. The two or more baseline shapes are ‘morphed’ together by first establishing a one-to-one correspondence between the shapes via some systematic shape collocation methods in either the functional[42] or geometric space[43,44]. The new shapes can then be generated by applying weights to the baseline shape collocation vectors and summing them together, essentially in a linear manner. The strength of DbM comes from the fact that it even works when the number of pre-existing designs are very small, e.g. around five[44], and can create an extensive design search space by means of ‘extrapolation’.

The DbM method is valid for shapes of any dimensions, and because radically different baseline shapes can be morphed together, exotic shapes can be created. Furthermore, as indicated above, in addition to ‘interpolation’ between the shapes, applying negative weights during morphing allows ‘extrapolation’ from the search space spanned by the baseline shapes, which can create truly novel and unusual shapes. Lastly, DbM is completely free from any geometric parameter constraints. The only implicit constraints are the selections of the ‘baseline shapes’ themselves, which are necessary to prescribe what problem is to be solved.

For 2D airfoils, the closed shapes can be collocated in the Euclidean coordinate system. We note here that all 2D shapes bounded by a single surface are homeomorphic to one another. Using the leading edge of each airfoil as origin, each shape can be collocated by taking fixed and uniformly spaced points on the  $x$ -axis, which creates a one-to-one correspondence between the shapes. This collocation strategy is demonstrated in Figure 1, and

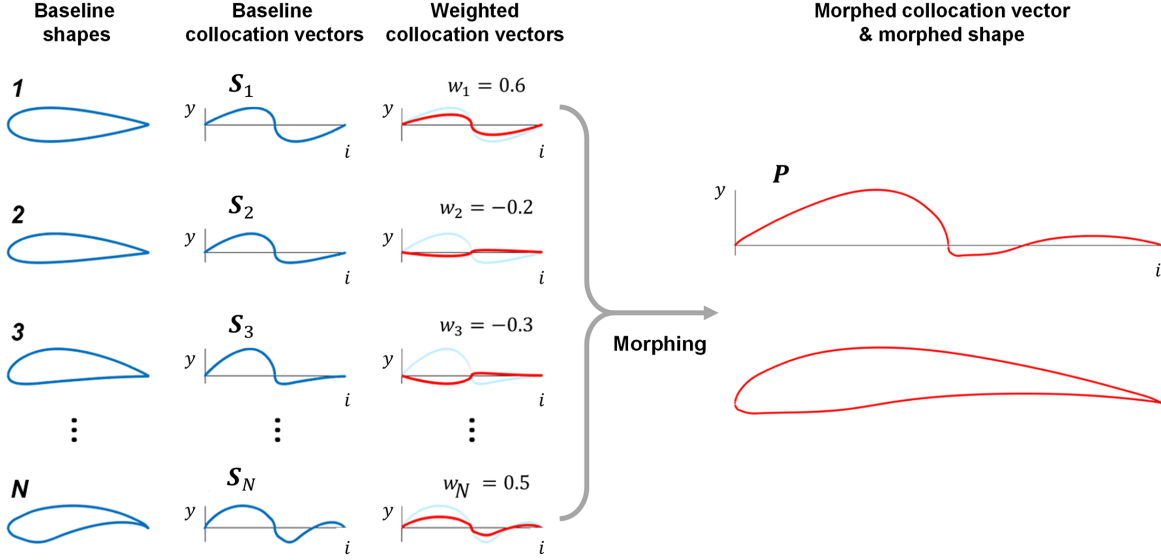


**Fig. 2** Application of DbM to 2D airfoils. Column 1 shows the baseline shapes. Column 2 depicts the elements of the collocation vectors of the baseline shapes plotted as a function of the index  $i$  of the collocation vector. Column 3 shows the weighted elements of the collocation vector plotted as a function of the index  $i$  of the collocation vector. Column 4 shows the resultant collocation vector of the morphed shape and the morphed shape itself.

the baseline shapes used in this paper are chosen from various airfoils from literature, which are detailed later. Morphing is performed by multiplying a specific airfoil shape with a scalar weight, summing up the weighted vectors, and then normalizing them, which is given by Eq. (1):

$$P(x) = \frac{1}{\sum_{m=1}^N w_m} \sum_{n=1}^N w_n S_n(x). \quad (1)$$

Here  $S_n(x)$  is the  $y$ -coordinate collocation vector determining the  $n^{\text{th}}$  baseline shape, collocated at  $x = [x_0, \dots, x_F]$  where the  $i^{\text{th}}$   $x$ -coordinate  $x_i = |1 - 2i/F|$  and  $F$  is the number of collocation points. Accordingly, the first half elements of  $S_n$  represents the top surface of the airfoil and the second half elements of  $S_n$  renders the bottom surface of the airfoil.  $N$  is equal to the total number of baseline shapes.  $w_n \in [-1, 1]$  is the morphing weight applied to the  $y$ -coordinate vector of the  $n^{\text{th}}$  baseline shape. A visual demonstration of our strategy is presented in Figure 2.

**2.2 Intersection Control.** For smooth baseline shapes, applying positive weights, i.e. interpolation, will always create smooth shapes without applying any geometric constraint. However, because the DbM imposes no geometric parameter restraints, extrapolation, i.e. applying negative weights, may produce non-physical geometries such as self-intersections, which have ‘zero-area’ regions as shown in Figure 3(a). One may discard the morphed airfoil shapes with self-intersections during the optimization but that diminishes the size of our design space. Instead, we recover new shapes by removing the intersections. This is accomplished by first locating within the morphed coordinate vector where the intersection occurs and restructuring the coordinate vector by ‘flipping’ it between the intersection points as shown in Figure 3(c). The vector is then ‘stiffened’ to remove the zero area between the intersections by removing the points in their neighborhoods and then linearly interpolating between the broken coordinate vectors. As seen in Figure 3(d), this removes the ‘zero-area’ space and gives some physical area to the shape at the point of intersection. The above process is repeated until all intersections are removed, e.g. both intersections in Figure 3 are successfully removed, and, finally, a moving-average smoothing filter is applied to smooth out the sharp edges.

**2.3 Baseline Shape Selection.** The selection of baseline shapes is an important component of DbM strategy and ultimately determines the size and the novelty of our search space. Metaphorically, the selection of the baseline airfoil shapes serves as the gene pool for the morphed airfoils, and its diversity is important for creating a large design space. Our baselines shape selection contains good ones with either high lift-to-drag ratio or good stall performance, bad ones with poor aerodynamic performance, commonly used airfoil shapes in the literature or industry, and airfoils with irregular shapes to provide novelty to the design space. It is worth noting that, contrary to the conventional airfoil optimization processes[46], we deliberately include the bad performers so that our optimization can suppress their features by assigning negative weights to the corresponding baseline shapes. Our results in later sections will demonstrate this in greater detail.

In this paper, we select 25 baseline shapes (see Figure 4) from the UIUC airfoil coordinates database[47]. The airfoils are selected to ensure diversity and to introduce radical features in the design space. Their model names and characteristics are attached in Appendix B. Each airfoil shape is represented by 4,000 coordinates that span from the first surface trailing edge around the leading edge to the second surface trailing edge with equally distributed  $x$ -coordinates parallel to the airfoil chord line of a unit length.

We note here that we deliberately do not adopt any quantitative approach to choose baseline shapes for DbM, such as selecting basis functions using POD [29–31] or SVD [32,33]. Although these techniques can work for airfoil design due to the availability of a large representative data set, for a wide range of engineering shape optimization problems, such datasets are rarely available and only a few baseline designs are present in the literature [42,44]. DbM is a general-purpose design technique which is applicable to such problems. We tend not to use any data-driven outcome that can be achieved from the huge existing database as input of DbM since it would become too problem-specific. Thus the baseline airfoil shapes are chosen qualitatively, with commonly used airfoils chosen from the UIUC database along with some radical shapes. Future efforts will be focused on sensitivity analysis of the DbM strategy to the choice of baseline shapes.

**2.4 Representation Capacity.** To examine the robustness and representation capacity of our design space generated by the mor-

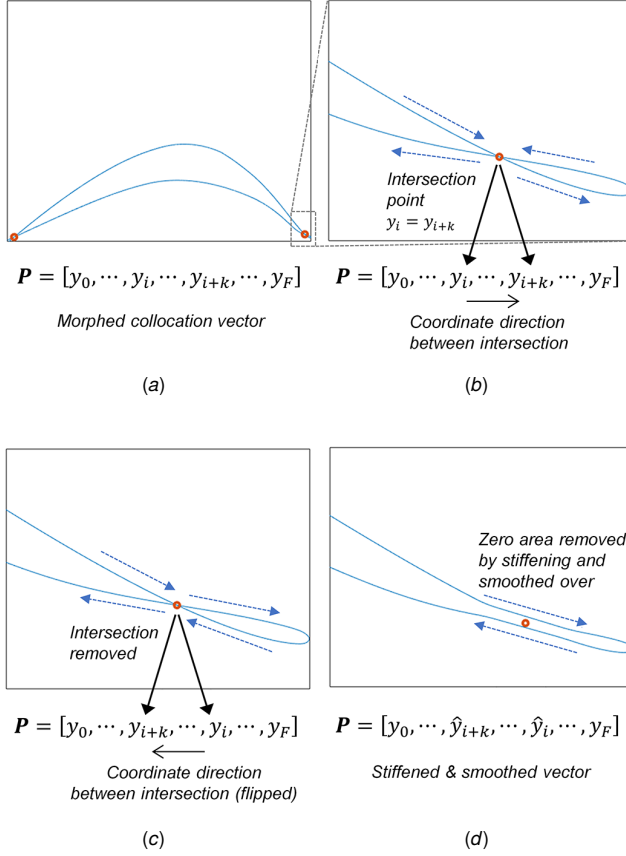


**Fig. 3 Conditioning for intersection removal. (a) Intersections are detected; (b) Blown up image of one intersection. Shape coordinates direction is depicted by arrows; (c) Intersection removed by flipping vector between intersection; (d) Zero area removed by linear interpolation to remove the intersecting area and then smoothed over, shown by hatted y-coordinates.**

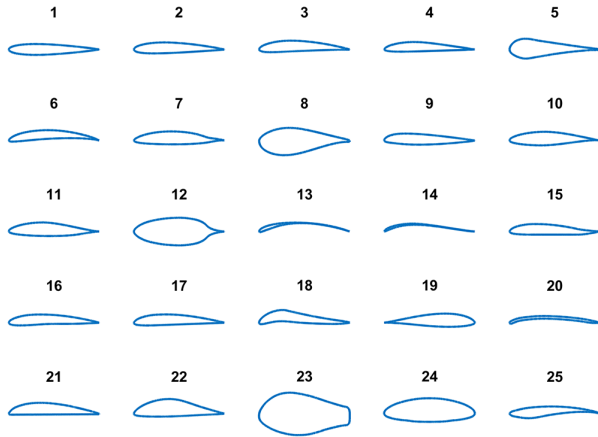


**Fig. 4 Twenty-five baseline shapes picked from the UIUC airfoil coordinates database[47]. See Appendix B for more details.**

phing of only 25 airfoil baseline shapes, we reconstructed the entire 2D airfoil shapes archived in the UIUC airfoil database[47] via DbM. For comparison purposes, we performed the same reconstruction with 3 conventional design methods commonly used airfoil parameterization: PARSEC[18], NURBS[23] and the Hicks-Henne approach[34], and compared the results.

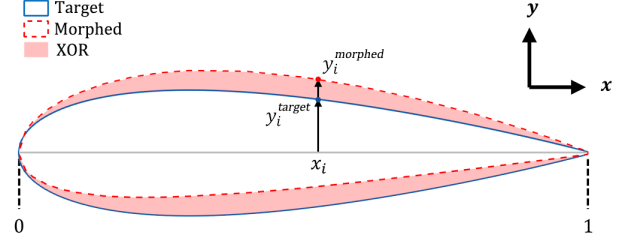


**Fig. 5 Geometric XOR of two similar airfoil shapes**

A total of 1,620 airfoils existing in the UIUC database were examined. For each airfoil reconstruction test, we attempted to find the closest morphed shape to the target one by running a global optimization of the input design parameters that minimizes representation error or XOR error. XOR is defined as the total area of the target and morphed shapes where one shape does not overlap with the other. An example is shown in Figure 5. Using the functional expression of an airfoil  $y(x_i) = y_i$  ( $0 \leq i \leq F$ ) as introduced in Figure 1(a), the geometric XOR may be understood as the collective difference in  $y$  between the target and morphed shapes.

$$\text{XOR}(\text{target}, \text{morphed}) = \frac{2}{F} \int_0^F y_i^{\text{error}} di, \quad (2)$$

where  $y_i^{\text{error}} = |y_i^{\text{morphed}} - y_i^{\text{target}}|$ . This error evaluates the similarity between 2 shapes since it gradually goes to zero as the shapes become identical to one another. When it is expressed in percentage terms, i.e.  $(\text{XOR} \times 100) \%$ , it emphasizes that the error is described as a proportion of the areal difference to the chord length squared. In our current case, all airfoil shapes are normalized to maintain a unit chord length.

For minimization of XOR, we utilized the MATLAB-based single-objective genetic algorithm. The population size was kept to 100, with maximum number of generations set at 500. The lower bound for XOR was set equivalent to  $1.44 \times 10^{-3}$  (or 0.144 %) from Eq. (2) for a chord length of 1. This is in accordance with the lower limit of Kulfan's typical wind-tunnel tolerance[35,48]. Accordingly, this value was selected as the lower bound of the optimization rather than zero for faster calculation. For comparison purposes, the same optimization scheme parameters were applied to all the airfoil design schemes tested here. DbM in this study uses 25 design parameters. Except for PARSEC where the design parameters are inherently fixed, we adhered to the methods where the number of the design variables are close to 25 for a rational comparison to the present DbM. Generally speaking, the fidelity of these design methods is improved as the number of design variables increases [48].

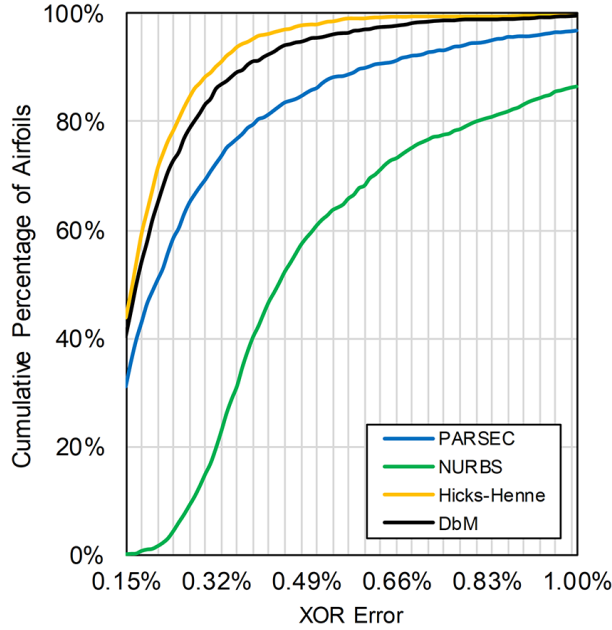
Applying DbM for reconstruction of the UIUC database, 1,611 airfoils, or 99.4% of the database, were reconstructed to < 1% XOR error. For the 9 other airfoils in the database, the DbM reconstruction still ended up achieving XOR error < 2%. Figure 6 exhibits the cumulative percentage of approximated airfoils, taking the UIUC database as the target, with respect to the error evaluated using the geometric XOR. Our DbM approach is found to be comparable to the Hicks-Henne approach and outperform the other two conventional airfoil shape parameterization methods.

We present 20 airfoil shapes obtained from each design method in Figure 7. To represent all 1,620 reconstructions, we first ranked the reconstructions in terms of the unweighted average of all XOR errors from the tested methods for each airfoil case and took our selections at every 5<sup>th</sup> percentile. Note that these 20 shapes are depicted in row-major order from the best one (NACA 651412) to the 95<sup>th</sup> percentile one (LA203A). It can be seen that NURBS often falls into the undesirable direction toward optimums where the upper and lower surfaces almost meet one another especially



**Table 1 Airfoil shape parameterization methods for comparison**

Method	Design Variables (DVs)	# of DVs	Remark
PARSEC	$r_{le}^{up/lo}$ : Leading edge radii	12	Fixed # of parameters
	$x^{up/lo}, y^{up/lo}$ : Crest coordinates		
	$y_{xx}^{up/lo}$ : Crest curvatures		
	$y_{te}, t_{te}$ : Trailing edge mid-position and thickness		
	$\alpha_{te}, \beta_{te}$ : Trailing edge direction and wedge		
NURBS	$x_{ctrl,i}^{up/lo}, y_{ctrl,i}^{up/lo}$ : Control point coordinates ( $i = 1, \dots, 4$ )	26	Third-order B-spline Evenly distributed knots
	$w_i^{up/lo}$ : Curve weights ( $i = 1, \dots, 4$ )		
	$y_{te}^{up/lo}$ : Trailing edge positions		
Hicks-Henne	$w_i^{up/lo}$ : Bump widths ( $i = 1, \dots, 6$ )	24	Base profile: NACA 0012 Cosine-distributed bump points
	$m_i^{up/lo}$ : Bump magnitudes ( $i = 1, \dots, 6$ )		
DbM (Present)	$w_i$ : Morphing weights ( $i = 1, \dots, 25$ )	25	See Figure 4 for the baselines


**Fig. 6 Cumulative percentage of approximated airfoils with respect to error measured by geometric XOR.**

around the leading edge. Even though this direction may help retain small XOR despite shape differences, it cannot ever reach perfect-zero. This observation explains the big failure of NURBS in the present comparison.

It is remarkable that DbM is competitive with the conventional methods in spite of the fact this technique is not specifically intended for airfoil parameterization. Compared to the other design strategies, DbM is applicable to wide range of problems and is extendable to higher physical dimensions. Even by qualitatively choosing baseline shapes without any data-driven basis selection, like the modal shape creation in POD, DbM is very competitive for reconstructing the UIUC database. Moreover, DbM's capability of creating exotic shapes via its extrapolation feature increases the chance to find novel solutions that are deviated from the previously-established space like the UIUC database. This exploration is

essential especially for the airfoil design where the correlation between the geometric feature and the aerodynamic performance of an airfoil can be very non-intuitive, thus necessitating exploratory design spaces.

One of the main way DbM is differentiated from the other methods is the ability to introduce novelty by simply adding a few novel baseline shapes. For other techniques, introducing such novelty would result in a significant increase in the number of design parameters. Baseline shapes that are considered "bad-performing designs" are deliberately included in the baselines. Even though these designs are evidently far from optima themselves, they may yield new chances to explore novel designs and therefore discover unexplored optimal designs especially because we allow extrapolation of the morphing. Let's consider for example baseline shape (#19), the 'flipped' airfoil in our DbM approach. It is considered off-design by the conventional methods that prescribe the airfoil geometry, e.g. fixing the relatively 'blunt' and 'sharp' edges at  $x = 0$  and  $x = 1$ , respectively, but not vice versa. This is evident when we try to reconstruct this airfoil using these techniques in Figure 8. For such methods, reconstructing this design well would require a significant increase in the number of design parameters whereas for DbM it requires just a single design parameter to introduce this novelty in. We believe this exploration is necessary for the present airfoil study where the correlation between the geometric feature and the aerodynamic performance of an airfoil is complicated and thus non-intuitive. Our final results will show that this 'flipped' airfoil has nontrivial contribution to the optimal airfoil shape formation via extrapolation (see Figure 12).

### 3 Optimization Methodology

Our airfoil optimization methodology is built around the DbM technique introduced in Sec. 2. As shown by the flowchart in Figure 9, the optimization starts from the selection of the baseline shapes and then evaluates and optimizes the airfoils formed by morphing these baseline shapes using DbM. Our methodology does not rely on one specific airfoil evaluation tool or one specific optimizer, and discussions on their choices are provided in Sec. 3.1 and Sec. 3.2 respectively.

**3.1 Airfoil Evaluation.** Our optimization methodology is not limited to one particular airfoil performance analyzer. One can use any reliable CFD or experimental methods. For the optimization

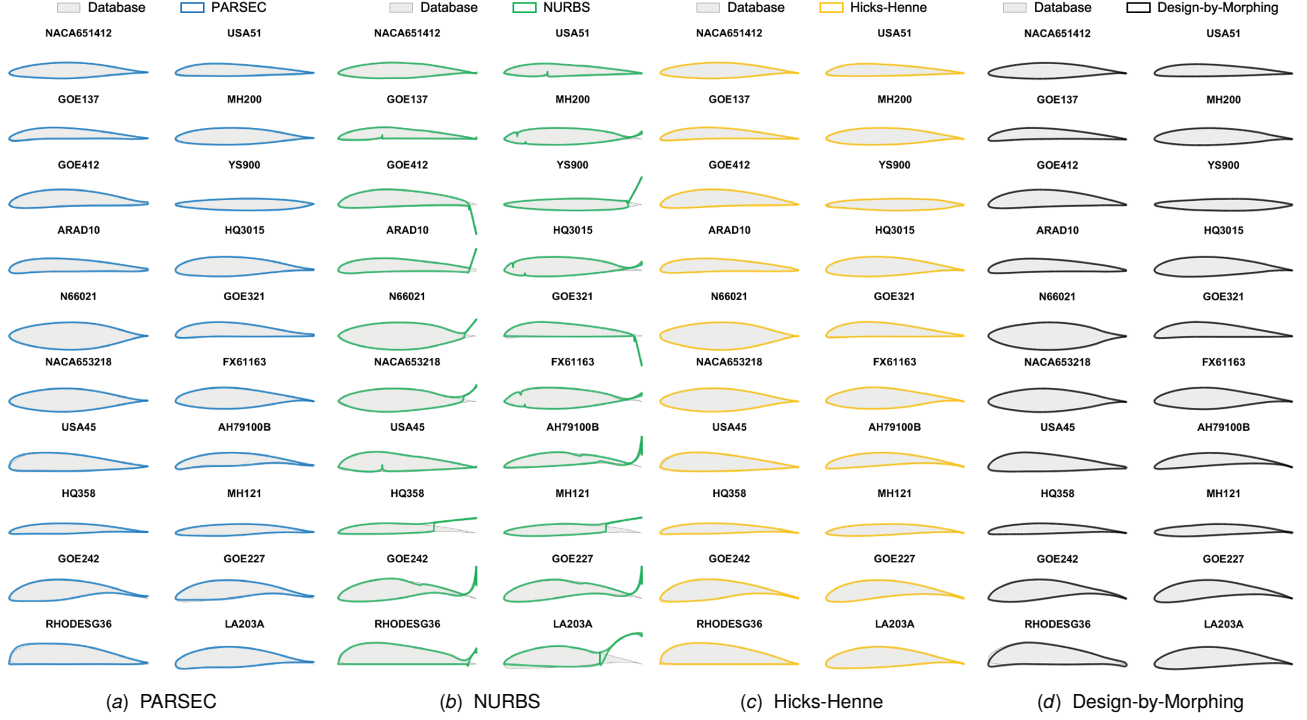


Fig. 7 Reconstruction of pre-existing airfoil shapes using different design parameterization methods.

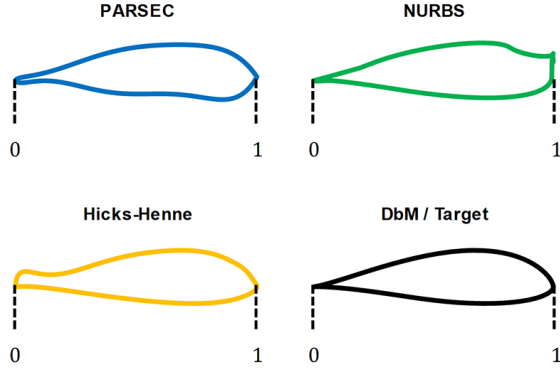


Fig. 8 Reconstruction of a deliberately “flipped” airfoil shape.

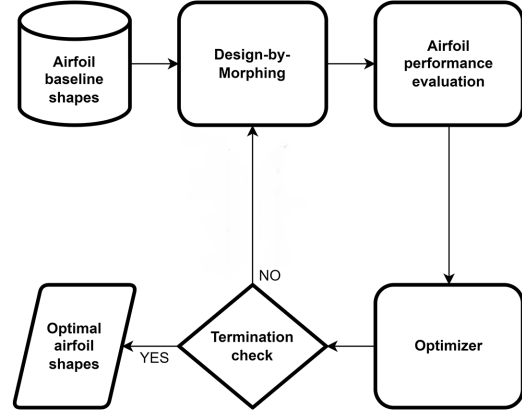


Fig. 9 General flowchart of airfoil optimization via DbM.

of airfoil shapes using CFD-based solvers, the evaluation of the objective functions (i.e. aerodynamic properties) typically falls into two categories: the full Reynolds-averaged Navier-Stokes (RANS) based approach and the interacted viscous/inviscid zonal approach. The RANS-based approach is computationally expensive and demands the optimizer to be highly efficient, and, to accommodate the large number of design variables as often seen in the aerodynamic designs, a gradient-based optimizer coupled with adjoint methods for computing the derivatives is deemed the most feasible[49–51]. On the other hand, the viscous/inviscid zonal approach, which combines separate solutions for the inviscid external flow and the viscous shear layer flow in an iterative manner to form a continuous profile, is faster and less expensive. Among a number of inviscid/viscous zonal airfoil analysis codes, XFOIL[52] has been the most dominant and widely adopted program[41,53–60]. It couples a vorticity panel method for exterior flow with an integral boundary-layer method for viscous boundary layers and uses

an  $e^9$ -type amplification formulation to determine the transition point[52]. Its applicability to airfoil designs has been demonstrated in the past literature, where its predictions of aerodynamic properties are shown in good agreement with the wind-tunnel experiment data[61,62] and the RANS-based simulation results[63].

The specific choice of the evaluation tool used in this paper is not essential to manifest the power of the DbM parameterization technique, which is the main focus of our paper. For this work, we opt for XFOIL because of its acceptable accuracy under our flow condition as well as its low computation cost. Its wide usage also allows quick reproduction of our optimization results. It is used in a black-box manner so that any other commercial or in-house airfoil analysis tools can be incorporated into our optimization framework if necessary. Our detailed airfoil evaluation setup is attached in Appendix B.

**3.2 Optimization.** When a set of solutions is given, the most optimal solution within the set can be determined without difficulty for single objective optimization problems, which is the case for most of the previous airfoil optimization studies [28,41,64]. However, for multi-objective optimization, multiple and potentially conflicting objectives must be considered simultaneously to determine the optimal answer in the solution set [65,66]. If the designer has a quantitative ranking of the objectives, these objectives can be combined together to formulate a single objective problem, but when no such ranking exists, constructing a Pareto front is the most common methodology [67–69], which is applicable to real-world problems such as the design of architected materials [70,71], turbomachinery [72–77], process-engineering [78–80], shape design [81–83], and structural engineering [84,85] when multiple objectives that cannot be quantitatively ranked are involved.

We pose the multi-objective optimization problem as

$$\mathbf{w}_{opt} = \underset{\mathbf{w} \in \mathcal{W}}{\operatorname{argmax}}(\mathbf{f}(\mathbf{w})), \quad (3)$$

where  $\mathbf{f}(\mathbf{w}) = [f_1(\mathbf{w}), f_2(\mathbf{w}), \dots, f_K(\mathbf{w})]$ . Here  $f_1, \dots, f_K$  are the  $K$  objectives to be maximized and  $\mathbf{w}$  is the design variable vector. Generally  $\mathbf{w}$  is a  $d$ -dimensional vector defined over a bounded set  $\mathcal{W} \subset \mathbb{R}^d$  representing  $d$  continuous variables.  $\{\mathbf{w}_{opt}\}$  is a set of Pareto-optimal solution vectors, i.e., a vector which is not Pareto-dominated by any other vector. For the reader's convenience, it is noted that a design variable vector  $\hat{\mathbf{w}}$  is Pareto-dominated by another design variable vector  $\tilde{\mathbf{w}}$  if  $f_k(\hat{\mathbf{w}}) \leq f_k(\tilde{\mathbf{w}})$  for all  $k \in \{1, \dots, K\}$ . To obtain the Pareto-front, especially when objectives cannot be weighted or when a non-convex black-box function is considered, evolutionary or genetic algorithms are a natural choice [80,86]. In fact, they have been commonly implemented in many previous aerodynamic optimization studies due to their gradient-free nature and wide region of the search domain [36,87–89]. On the other hand, when the cost functions are expensive to compute (e.g. when using experiments or CFD as an evaluation tool), Bayesian optimization methods have been proven to be efficient [90].

Our study considers a bi-objective ( $K = 2$ ) two-dimensional airfoil shape optimization. In particular, we optimize the shape of a subsonic airfoil operating in an incompressible flow with  $\operatorname{Re} \equiv Uc/\nu$  of  $1 \times 10^6$ , where  $U$  and  $\nu$  are the free-stream flow speed and fluid kinematic viscosity, respectively, and  $c$  is the airfoil chord length. The parameter to be optimized is the morphing weight vector for the DbM technique:

$$\mathbf{w} \equiv (w_1, \dots, w_{25}) \in \mathcal{D}^{25}, \quad (4)$$

where  $\mathcal{D} = [-1, 1] \subset \mathbb{R}$  and  $w_i$  ( $i = 1, 2, \dots, 25$ ) is the weight applied to the  $i^{\text{th}}$  baseline shape. The design objectives to be maximized are the maximum lift-drag ratio at any angle of attack  $\alpha$ , i.e.  $f_1(\mathbf{w}) = CLD_{max}(\mathbf{w})$ , and the difference between the stall angle  $\alpha_s$  and the angle where the maximum lift-drag ratio occurs, i.e.  $f_2(\mathbf{w}) = \Delta\alpha(\mathbf{w})$ , where  $\Delta\alpha$  is often called the stall angle tolerance. Precise definitions of these design objectives are explicated in Appendix A, and both objectives are evaluated using the XFOIL simulations, which are efficient enough to be used with the genetic algorithm. These objectives present an interesting combination for use in vertical-axis wind turbines [43].

We use a MATLAB-based variant of the popular NSGA-II [91] algorithm, which is a controlled, elitist genetic algorithm. Our initial population consists of the single-objective optimums of each design target as well as random samples in the design space. The population size of 372 is used with a total of 3,000 maximum generations, and the solutions are actively ranked within each generation so as to maintain diversity and avoid over-crowding in the Pareto-optimal solution set. Our setup was tested on the commonly used set of ‘ZDT’ benchmark problems for multi-objective problems, suggested by Zeidler et al. [92]. The details of the test problems and the validation results are provided in Appendix C.

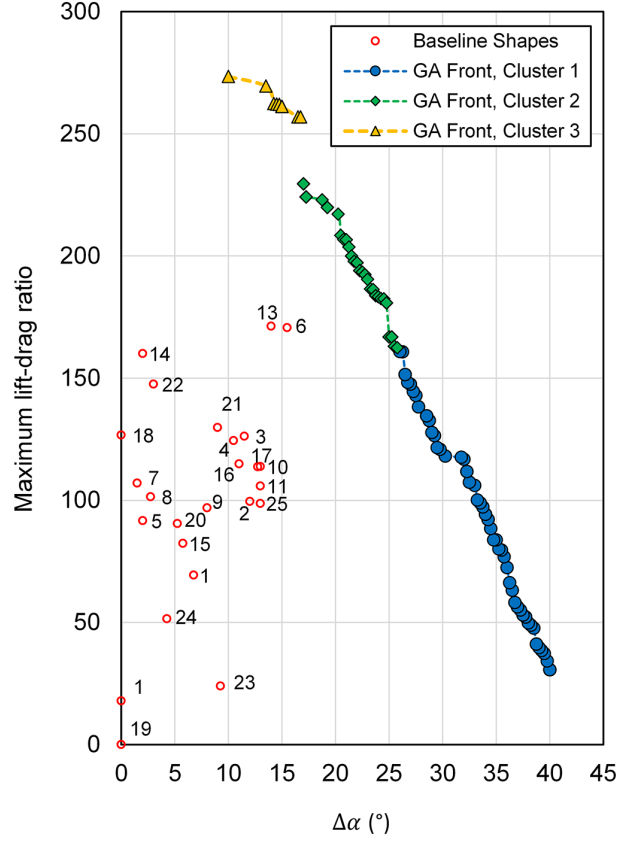


**Fig. 10** The Pareto front consisting of the optimal airfoil shapes as a result of the 3,000 generation runs of NSGA-II. Twenty-five red hollow circles with indices indicate twenty-five baseline airfoil shape evaluations. See Appendix D to understand how the clustering is performed.

## 4 Results

The Pareto front on the  $\Delta\alpha - CLD_{max}$  objective plane, which resulted from the 3,000 generation genetic algorithm (GA) runs, is depicted in Figure 10. The convergence of the front is confirmed by the large generation number with the population size of 372, involving around 1.1 million XFOIL evaluations of  $CLD_{max}$  and  $\Delta\alpha$ . A set of 208 Pareto-optimal airfoil shapes was obtained via DbM using 25 baseline airfoil shapes. For comparison, these 25 baseline shape cases are evaluated and plotted as red hollow circles in Figure 10 together. Baseline #19 has zero  $CLD_{max}$  and  $\Delta\alpha$  because we intentionally inverted the shape and therefore XFOIL failed to evaluate its aerodynamic performance. We assigned the objective functions zero values for such failing cases because they represented airfoil geometries that are not aerodynamically viable in the XFOIL space. The GA optimization successfully developed the Pareto front, where two ends are posed at  $(CLD_{max}, \Delta\alpha) = (30.63, 40^\circ)$  and  $(CLD_{max}, \Delta\alpha) = (273.39, 10^\circ)$ . Even in the largest maximum lift-drag ratio case, the angle of attack gap between stall and design point is found to be  $10^\circ$ , giving the airfoil a tolerant range for off-design operations.

The front is divided into 3 different clusters, each of which constitutes a segment of the front which does not overlapping one another. It is worth noting that the non-overlapping division of the front is a consequence of clustering through the Principal Component Analysis (PCA), rather than arbitrary. The detail of the clustering is provided in Appendix D.

Figure 11 shows nine representative optimal airfoil shapes on the Pareto front in ascending order of  $CLD_{max}$ . In each cluster, three airfoil shapes having considerably different objective function

values were selected to be presented. Also, note that Figure 11(a) illustrates the extreme case of the smallest  $CLD_{max}$  and largest  $\Delta\alpha$  while Figure 11(i) depicts the other extreme of the largest  $CLD_{max}$  and smallest  $\Delta\alpha$ . It can be seen that within the cluster the overall shape remains identical and only a gradual decrease in the airfoil thickness is observed as  $CLD_{max}$  increases. Since thin airfoils such as bird-like airfoils[93], which we take as part of the baseline shapes, e.g. #13 and #14, are known to have high  $CLD$  performance, the trend of airfoil thickness observed in the Pareto front appears to be reasonable.

In cluster 1 where 112 optimal airfoil shapes exist, it is found that they mostly look similar to the total mean airfoil shape, where the mean airfoil shape is the mean of all the airfoil shapes in the Pareto-front (see Figure 13(a)). This makes sense because they account for the majority of the airfoil shapes located on the front. Moreover, this cluster is located near the origin in the PCA-projected weight space (see Figure 16 in Appendix D), indicating that there was no radical morphing of the airfoil shape taking place from the mean shape.

Next, cluster 2 contains 83 optimal airfoil shapes. Compared to the airfoil shapes in cluster 1, the most distinguishing feature is that the trailing edge region becomes narrow. This creates the sharp trailing edge, which is generally favorable to obtain a lift increase. However, they are still not deviated far from the origin in the PCA-projected weight space, and their common shape mostly resembles the total mean airfoil shape.

Finally, 13 optimal airfoil shapes are discovered in cluster 3 from the optimization. This cluster includes the airfoil shapes experiencing more drastic morphing than the other clusters. It can be confirmed that they are the thinnest airfoils where the leading edge region's thickness is also diminished.

The mean weight distributions with respect to 25 original baseline shapes are given in Figure 12. Overall, the weight distributions of 3 clusters comply with the weight distribution of the total mean. It turned out that baseline shape #13 (model name: AS6097) is commonly the most significant one for morphing. Since this baseline shape is the best in  $CLD_{max}$  and the second best in  $\Delta\alpha$  among 25 baseline shapes (see Figure 10), it was likely to survive in the GA runs over the generations against the selection pressure that only sorts out dominant individuals in terms of both  $CLD_{max}$  and  $\Delta\alpha$ . However, excellence in the objectives of an individual baseline shape does not necessarily guarantee its survival, which is the case for the globally best baseline shape #6 (model name: AH 79-100C), as an individual's superior 'phenotype' may be no longer revealed, or even suppressed after the morphing is done and all 'genes' are mixed with each other. In the same sense, inferiority in the objectives of an individual does not anticipate its elimination in the end (e.g. the 'flipped' baseline #19).

As we discussed from the examination of the morphed airfoil shapes, both cluster 1 and 2's mean weight distributions show no considerable difference from the total mean weight distribution. Through small shape variation from the total mean airfoil shape as in Figure 13(a), it is possible to reach these optima relatively easily. In contrast, cluster 3 has a number of weights that are quite different from the mean (e.g., #6 and #11) and substantial morphing would be required if one starts with the total mean airfoil shape.

In the context of the present study, each axis obtained by the PCA can be represented by a unique form of morphed airfoil shape because 25 PCA coefficient vectors defined in the weight space  $\mathcal{D}^{25}$  are orthogonal to each other. These 25 new morphed airfoils span the whole design space and therefore serve as alternative baseline shapes in lieu of the original ones. More importantly, the dominance of the first 2 PCA axes with respect to the data point variance suggests that the major geometric feature of 208 airfoil shapes we found via the optimization is virtually generated by morphing of these two new airfoils. Small variance of a PCA axis indicates that the data points are not considerably deviated from their mean on the axis. In other words, the baseline shape corresponding to this PCA axis has an marginal impact on morphing the airfoil shape

for optimization. Once we pick two baseline shapes from the first two dominant PCA axes, whose associated collocation vectors are say  $P_1$  and  $P_2$ , and use them to morph the airfoil shape obtained from the total mean of the Pareto-optimal weight vector set, which corresponds to the mean collocation vector  $P_{mean}$ , we get better understanding of how the morphing, especially along each PCA axis, has an influence on major geometric changes in the optimal airfoil shapes. These airfoil shapes are depicted in Figure 13, where the black and red surfaces are generated from the first and second half of the collocation points, respectively. For example, we note that the orientation of two surface of  $P_1$  is flipped in comparison to that of  $P_{mean}$ , meaning that the stronger the weight of PCA axis 1 in the positive direction is, the narrower a morphed airfoil shape is.

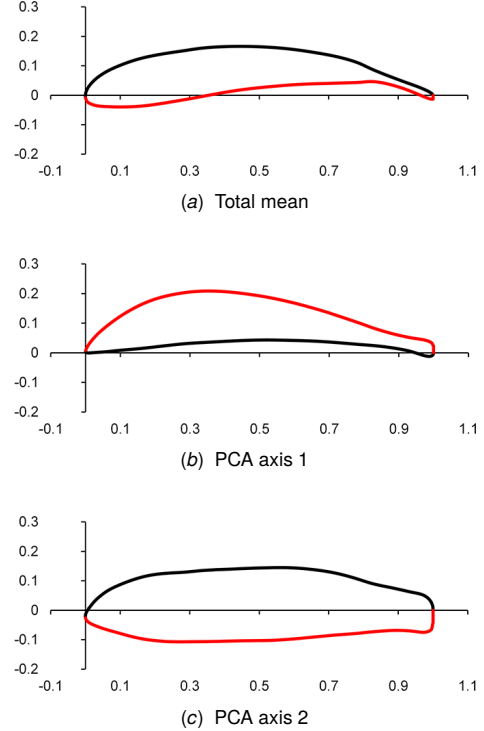


**Fig. 13 Morphed airfoil shapes generated by the optimal weight vectors, representing (a) the total mean of all optimal airfoils' weights, (b) the coefficients of the PCA axis having the most variance and (c) the coefficients of the PCA axis having the second-most variance. The black and red surfaces correspond to the first and second half of the collocation points, respectively.**

## 5 Discussion

Most parameterization strategies depend upon careful selection of constraints and parameters, which determines their probability of success. The fidelity offered by such methods is highly dependent on the number of the parameters chosen. Moreover, these designs are limited by the parametric constraints and the implicit designer's bias, making extrapolation or radical global changes difficult. Data driven methods typically rely on the assumption that the optimum solutions are not far from the training data-set, which again prevents radical shape changes.

DbM, on the other hand, creates a design space that is uninhibited by any geometric constraints, allows extrapolation from the design space which is useful especially for airfoil design, and is applicable to a wide range of engineering design problems. It doesn't suffer from the curse of dimensionality when parameterizing air-



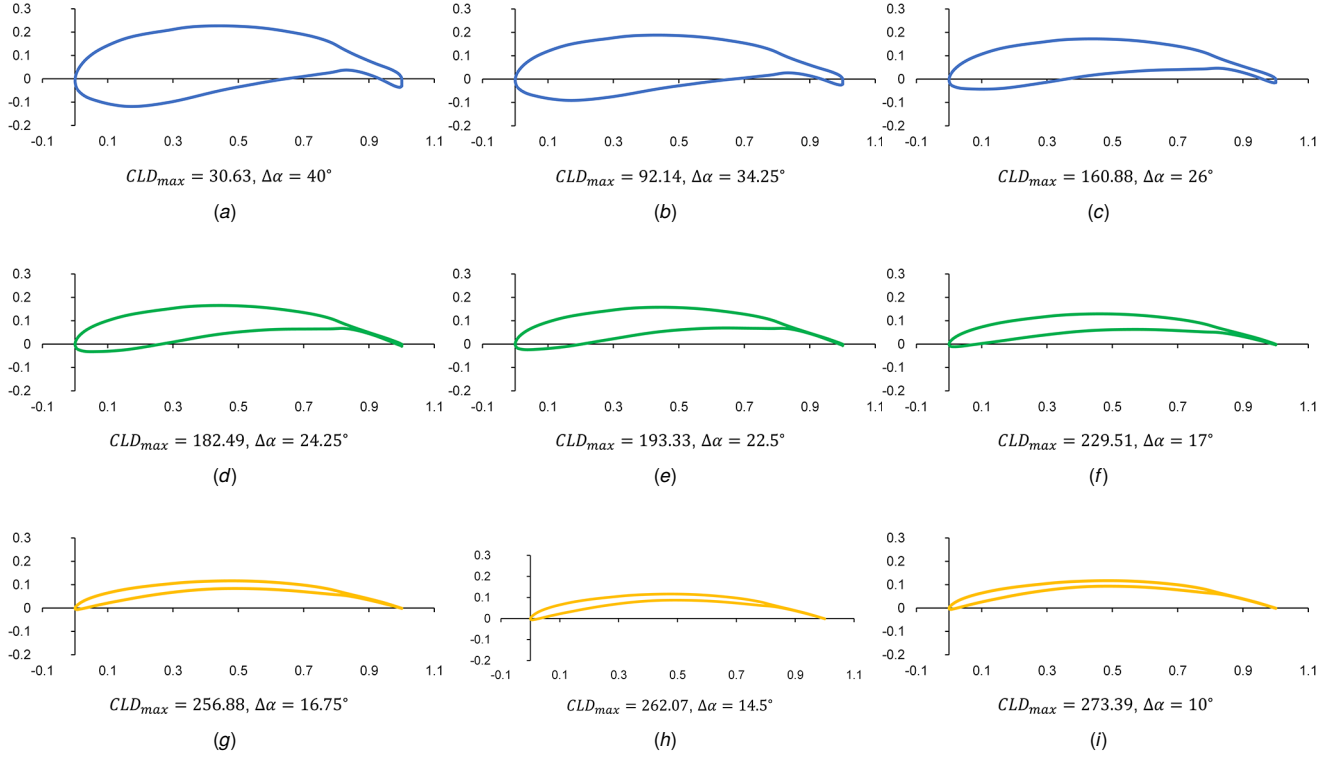


**Fig. 11** Nine representative Pareto-optimal airfoil shapes. (a)-(c) are in cluster 1, (d)-(f) are in cluster 2 and (g)-(i) are in cluster 3.

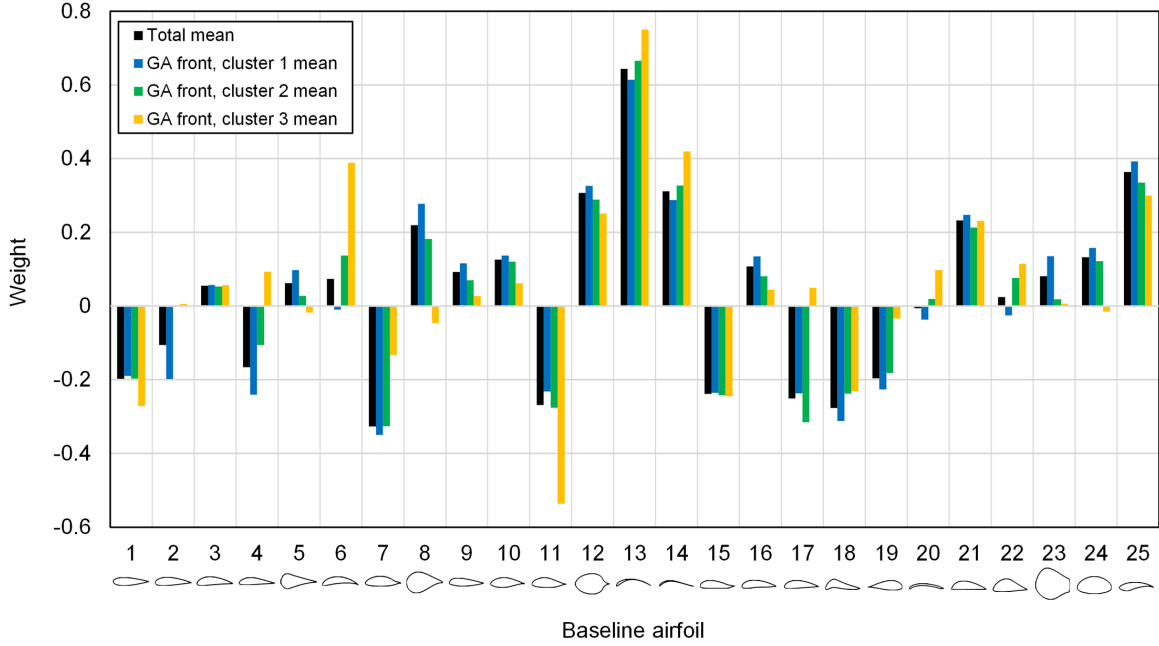


**Fig. 12** Mean weight distributions of the Pareto-optimal airfoil shapes with respect to twenty-five baseline airfoil shapes.

foils and allows high-fidelity representation of airfoils without increasing the number of independent parameters in the problem. Using only 25 baseline shapes from the UIUC database, we were able to recreate 99.4% of UIUC database with < 1% error. We also showed that radical, global changes are possible using DbM. Applying that for the bi-objective shape optimization with objectives of maximizing  $CLD_{max}$  and  $\Delta\alpha$ , we were able to achieve significant results compared to our baseline shapes. We posit that,

for design parametrization of airfoils and for other 2D/3D shapes, DbM should be the method of choice for creating an unconstrained, unbiased and non-data intensive design space that allows radical modifications, which can often be non-intuitive shapes. In this paper, our qualitative selection of 25 baseline shapes satisfactorily spanned the design space with tolerable error. However, it would be possible that even a smaller number of baseline shapes than 25 successfully construct the design space if some of the current

baseline shapes were redundant. For better understanding of DbM, our future work would focus on performing sensitivity analysis of DbM on baseline shape selection and developing a more rigorous method for choosing DbM baselines.

## 6 Conclusion

The DbM methodology creates a design space for radical 2D airfoils. We show that the space creates novel airfoils that are not constrained by geometric parameters or designer bias. Optimizing the design space created for dual objectives of  $CLD$  and  $\Delta\alpha$ , we show remarkable improvements in both objectives and provide a Pareto-front of optimal airfoil designs. Our final airfoils show remarkable improvements over our existing baseline shapes. For optimizing 2D or 3D airfoils, DbM should be used as the method of choice for design space creation. Moreover, our methodology is flexible to be used for optimizing shapes for other fluid machinery as well. Currently we are applying DbM in tandem with Bayesian optimization for the optimization of 3D airfoils and vertical-axis wind turbines.

## Acknowledgment

The authors would like to thank Dr. Ömer Savaş, affiliated with the Department of Mechanical Engineering, University of California at Berkeley for insightful discussions regarding airfoils and aerodynamics. The authors would also like to acknowledge that this work used the Extreme Science and Engineering Discovery Environment (XSEDE), which is supported by National Science Foundation grant number ACI-1548562 through allocation TG-CTS190047.

## Funding Data

No funding was received for the undertaking of this project.

## Data and Materials Availability

The data needed to evaluate the conclusions are present in the paper and Appendices. The data files and optimization setup will be posted in a public repository upon publication of the paper.

## Nomenclature

- $c$  = airfoil chord length (m)
- $d$  = drag force of an airfoil per unit span ( $\text{N m}^{-1}$ )
- $l$  = lift force of an airfoil per unit span ( $\text{N m}^{-1}$ )
- $\mathbf{P}$  = y-coordinate collocation vector of a morphed airfoil
- $\mathbf{S}$  = y-coordinate collocation vector of a baseline airfoil
- $U$  = free-stream flow speed ( $\text{m s}^{-1}$ )
- $w$  = design-by-morphing weight factor

## Greek Letters

- $\alpha$  = airfoil angle of attack ( $^\circ$ )
- $\alpha_s$  = airfoil stall angle ( $^\circ$ )
- $\Delta\alpha$  = stall angle tolerance, the range of  $\alpha$  between the stall point and the maximum lift-drag ratio point ( $^\circ$ )
- $\nu$  = fluid kinematic viscosity ( $\text{m}^2 \text{s}^{-1}$ )
- $\rho$  = fluid density ( $\text{kg m}^{-3}$ )

## Dimensionless Groups

- $C_d$  = drag coefficient of an airfoil per unit span,  $2l/(\rho U^2 c)$
- $C_l$  = lift coefficient of an airfoil per unit span,  $2d/(\rho U^2 c)$
- $CLD$  = lift-drag ratio of an airfoil,  $C_l/C_d$
- $CLD_{max}$  = maximum lift-drag ratio of an airfoil,  $\max_{\alpha} CLD(\alpha)$
- Re = Reynolds number based on airfoil chord length,  $Uc/\nu$

## Appendix A: Aerodynamic Optimization Objectives

Airfoil optimization has become common in aerodynamic design problems involving maximization of one or more performance parameters of an airfoils. We mainly consider the following 2 performance parameters: the lift-drag ratio and stall angle. Given the flow speed  $U$ , fluid density  $\rho$  and airfoil chord length  $c$ , the lift and drag coefficients of an airfoil per unit span at an angle of attack  $\alpha$ ,  $C_l$  and  $C_d$ , are expressed as

$$C_l(\alpha) \equiv \frac{l(\alpha)}{\frac{1}{2}\rho U^2 c}, \quad C_d(\alpha) \equiv \frac{d(\alpha)}{\frac{1}{2}\rho U^2 c} \quad (\text{A1})$$

where  $l$  and  $d$  are lift and drag force per unit span, respectively, both of which change with respect to  $\alpha$ . In this paper, these parameters are predicted via XFOIL[52], an program for analysis of subsonic isolated 2D airfoils, with varying  $\alpha$  and then used for the optimization. Based on  $C_l$  and  $C_d$ , the lift-drag ratio  $CLD$  is calculated as:

$$CLD(\alpha) = \frac{C_l(\alpha)}{C_d(\alpha)}. \quad (\text{A2})$$

On the other hand, we define the stall angle  $\alpha_s$  as an angle of attack where  $C_l$  reaches the first local maximum when we increase the angle starting from  $0^\circ$ , or

$$\alpha_s \equiv \min_{\alpha \geq 0} \alpha \quad \text{where} \quad \exists \delta > 0 \quad \text{such that} \quad (\text{A3})$$

$$C_l(\alpha) \geq C_l(x) \quad \forall x \in [\alpha - \delta, \alpha + \delta]$$

Note that this definition is more conservative than the typical definition of the stalling in practice, where flow at the rear region begins to fully separate and  $C_l$  is globally maximized.  $\alpha_s$  is occasionally smaller than the global maximum of  $C_l$ . Nonetheless, this approach helps avoid overestimation of the stall angle, which is expected to happen in XFOIL because of the nature of its flow solver having a limited accuracy in stall and post-stall conditions.

$CLD$  and  $\alpha_s$  have been typically considered to be significant to characterize the airfoil performance. For example, when it comes to lift-type wind turbines, the point where  $CLD$  is maximized may be commonly chosen as the design point. Since a wind turbine cannot always operate in the design condition, however,  $\alpha_s$  needs to be additionally considered to evaluate how far the turbines run under an increasing-lift condition. For well-designed airfoils,  $\alpha_s$  generally occurs later than the design point, which yields tolerance in operation beyond the design point. Consequently, the stall angle tolerance, i.e. the range between these two angles of attack  $\Delta\alpha$ , which is expressed as

$$\Delta\alpha \equiv \max_{\alpha \in \mathbb{R}} \left( 0, \alpha_s - \arg\max_{\alpha} CLD(\alpha) \right), \quad (\text{A4})$$


























can be a proper choice to evaluate the off-design performance [94]. Figure 14 depicts a scheme of how  $CLD$  and  $\Delta\alpha$  are determined on performance curves of an airfoil.

## Appendix B: Baseline Airfoil Shapes and Validation

Our optimization methodology does not rely on one specific airfoil evaluation tool. To compare our results with the previous literature and to help future researchers quickly reproduce our results, we use XFOIL[52] in the present study. The two design objectives,  $CLD_{max}$  and  $\Delta\alpha$ , are obtained from the  $C_l$  and  $C_d$  data calculated by the XFOIL at different angle of attacks (see Figure 14).

To achieve better efficiency and consistency, we only use the XFOIL to generate the performance data and do not use any of its built-in paneling features. The conditioning and the re-paneling of the morphed airfoil coordinates are handled at the end of our DbM

**Table 2** The model names, features, shape outlines, and XFOIL evaluation results of the 25 baseline shapes used by DbM in this paper. The coordinates of the baseline shapes are obtained from the UIUC airfoil coordinates database[47]. The airfoil evaluation results are obtained for an incompressible outer-flow of  $Re = 1 \times 10^6$ . The reference evaluation results are interpolated from the Airfoil Tools online database[95], where N/A indicates that there is no data available for this airfoil.

Index	Model Name	Series (Features)	Airfoil Shape	Reference[95]		Present	
				$CLD_{max}$	$\Delta\alpha$	$CLD_{max}$	$\Delta\alpha$
1	NACA 0012	NACA (4-digit)		75.6	8.50	69.3	6.75
2	NACA 2412	NACA (4-digit)		101.4	12.00	99.5	12.00
3	NACA 4412	NACA (4-digit)		129.4	1.75	126.2	11.50
4	E 205	Eppler		128.3	8.50	124.4	10.50
5	AH 81-K-144 W-F Klappe	Althaus		89.7	2.00	91.6	2.00
6	AH 79-100 C	Althaus		183.0	14.75	170.6	15.50
7	AH 79-K-143/18	Althaus		110.9	1.50	107.0	1.50
8	AH 94-W-301	Althaus		103.0	4.00	101.4	2.75
9	NACA 23112	NACA (5-digit)		98.6	6.75	96.9	8.00
10	NACA 64(2)-415	NACA (6-digit)		120.6	12.50	113.8	13.00
11	NACA 747(A)-315	NACA (7-digit)		111.5	12.00	105.8	13.00
12	Griffith 30% Suction	Griffith (Suction)		17.3	0.00	17.9	0.00
13	AS 6097	Selig (Bird-like)		N/A	N/A	171.2	14.00
14	E 379	Eppler (Bird-like)		N/A	N/A	160.0	2.00
15	Clark YS	Clark		85.7	5.25	82.3	5.75
16	Clark W	Clark		116.1	11.00	114.8	11.00
17	Clark Y	Clark		114.8	11.75	113.7	12.75
18	Chen	Chen		125.4	0.00	126.7	0.00
19	S2027 Flipped	Selig (Flipped)		N/A	N/A	0.00	0.00
20	GOE 417A	Gottingen (Thin plate)		86.7	5.25	90.4	5.25
21	GOE 611	Gottingen (Flat bottom)		125.6	9.00	129.7	9.00
22	Dragonfly Canard	Dragonfly		144.6	2.50	147.5	3.00
23	FX 79-W-470A	Wortmann (Fat)		N/A	N/A	23.9	9.25
24	Sikorsky DBLN-526	Sikorsky (Fat)		53.3	4.75	51.5	4.25
25	FX 82-512	Wortmann		99.1	14.75	98.7	13.00

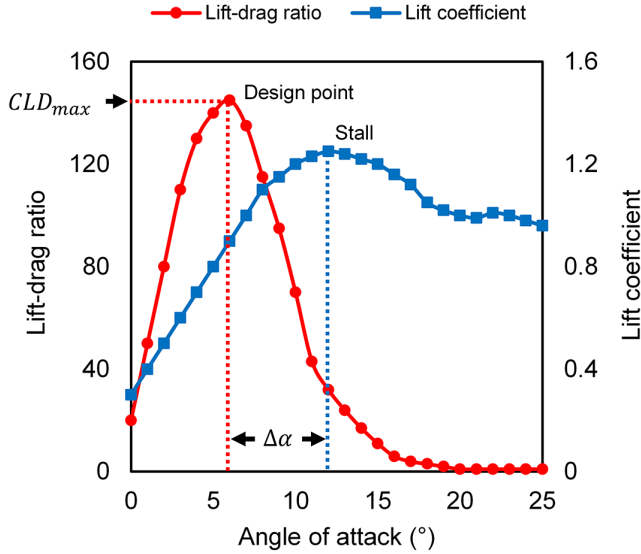


**Fig. 14** Airfoil performance curves.

algorithm. To reduce the evaluation time, we perform a rough scan first with an  $\alpha$  increment of  $1^\circ$  and then finer scans for  $CLD_{max}$  and  $\Delta\alpha$  separately with an  $\alpha$  increment of  $0.25^\circ$ .

It is worth noting that XFOIL uses a global Newton's method[52] to simultaneously solve for the boundary layer and the transition equations, and it uses the solution at the previous angle of attack as the starting guess. As a result, ill-conditioned airfoil coordinates and the occurrence of the flow separation can both lead to the non-convergence of the XFOIL evaluation. To ensure the robustness and correctness of our airfoil evaluation, our XFOIL wrapper attempts to reach convergence by re-starting the root-finding with a fresh starting guess and by gradually increasing the number of the panels. If both attempts fail, the wrapper will check the convergence at the neighboring points, which will indicate whether the flow separation occurs or not. Besides the non-convergence issue, we further verify the correctness of the Newton's method by comparing the calculated viscous drag coefficient and the inviscid drag coefficient, the later of which is determined purely by the potential flow theorem and have to be smaller than its viscous counterpart due to its negligence of the friction (viscous effect). Any angle with incorrect result will undergo the same treatment as the non-converging ones, hence ensuring the correctness of our airfoil performance evaluation. A comparison between our XFOIL evaluation and the past experimental results of the same airfoil under the same flow conditions is provided in the table.

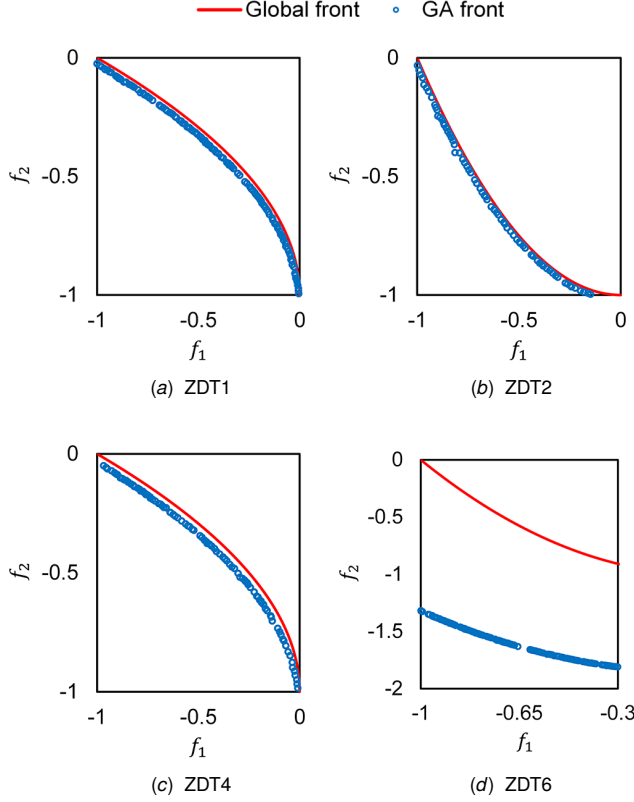


Fig. 15 Multi-objective optimization of benchmark test functions using GA.

### Appendix C: Optimization Test Functions and Validation

We use the multi-objective problems, suggested by Zeidler et al.[92], for testing our GA setup. The details of the test functions are given in Table 3. All the test functions were minimized with 25 variables in the design space.

MATLAB’s NSGA-II genetic algorithm, a fast sorting and elitist multi-objective genetic algorithm, was used in the current study. Single objective optimization for each objective and random sampling were used for initialization. The population size of 372 was used with a total of 3,000 maximum generations. A ‘phenotype’ crowding distance metric was used. This setup was validated on the test functions described above. All the problems were benchmarked with 25 variables ( $d = 25$ ) and two objective functions ( $K = 2$ ) as with the present airfoil optimization problem. The results of our setup on four benchmark problems are shown in Figure 15. It was found that the algorithm could capture ZDT1, ZDT2, and ZDT4 accurately and predicts ZDT6, which is not only non-convex but also non-uniform, reasonably well.

### Appendix D: Airfoil Shape Clustering

To analyze characteristics of the optimized airfoil shapes in detail, the airfoil shapes on the Pareto front are classified into 3 clusters using  $k$ -means clustering based on the Euclidean distance with  $k = 3$ . The clustering is performed in the design variable space, or weight space, of  $\mathcal{D}^{25}$  rather than in the objective plane because the purpose of clustering is to identify common geometric features over different airfoil shapes as a result of the optimization. The selection of the cluster size is based on the PCA of the optimal weight vector set.

We note here that the baseline shapes chosen might be linearly dependent. The distances in the PCA weight space, thus, might not be rigorous as a morphed shape on the Pareto-front may be

represented by another set of weights. However, the PCA analysis is used only to identify if qualitative classes within the Pareto-front could be found and clustered together and to glean some additional insights of our Pareto-front results.

Figure 16 shows the projection of the 25-dimensional weight vector set to the 2-dimensional subspace spanned by 2 PCA axes having the first- and second-most variance. The explained variance ratios of PCA axes 1 and 2 are 77.8% and 14.6%, respectively. On the other hand, the PCA axis of the third-most variance accounts for only 2.5% of the variance, affirming that the 2-dimensional projection in Figure 16 adequately scatters the clusters. From this observation,  $k = 3$  is thought to be the most appropriate cluster size.

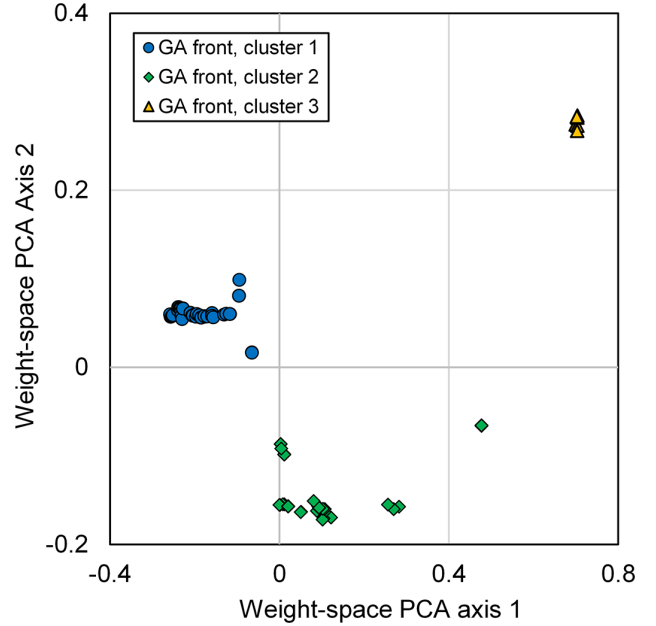


Fig. 16 Projection of the 25-dimensional optimal weight vectors to the 2-dimensional subspace spanned by 2 PCA axes of the dominant variance.  $k$ -means clustering with the cluster size of 3 is used to identify the clusters.



**Table 3 Benchmark Test Functions.** All of the test functions are bi-objective with extended to  $n$ -dimensional constrained search space.

Problem	Bounds	Objective Functions	Optima	Note
ZDT1	$w_i \in [0, 1],$ $i = 1, \dots, n$	$f_1(\mathbf{w}) = w_1$	$w_1 \in [0, 1]$ $w_i = 0,$ $i = 2, \dots, n$	convex
		$f_2(\mathbf{w}) = g(\mathbf{w}) \left[ 1 - (f_1(\mathbf{w})/g(\mathbf{w}))^{1/2} \right]$		
		$g(\mathbf{w}) = 1 + 9 \left( \sum_{i=2}^n w_i \right) / (n-1)$		
ZDT2	$w_i \in [0, 1],$ $i = 1, \dots, n$	$f_1(\mathbf{w}) = w_1$	$w_1 \in [0, 1]$ $w_i = 0,$ $i = 2, \dots, n$	non-convex
		$f_2(\mathbf{w}) = g(\mathbf{w}) \left[ 1 - (f_1(\mathbf{w})/g(\mathbf{w}))^2 \right]$		
		$g(\mathbf{w}) = 1 + 9 \left( \sum_{i=2}^n w_i \right) / (n-1)$		
ZDT4	$w_1 \in [0, 1]$ $w_i \in [-5, 5],$ $i = 2, \dots, n$	$f_1(\mathbf{w}) = w_1$	$w_1 \in [0, 1]$ $w_i = 0,$ $i = 2, \dots, n$	non-convex
		$f_2(\mathbf{w}) = g(\mathbf{w}) \left[ 1 - (f_1(\mathbf{w})/g(\mathbf{w}))^{1/2} \right]$		
		$g(\mathbf{w}) = 10n + \sum_{i=2}^n \left( w_i^2 - 10 \cos(4\pi w_i) \right) - 9$		
ZDT6	$w_i \in [0, 1],$ $i = 1, \dots, n$	$f_1(\mathbf{w}) = 1 - \exp(-4w_1) \sin^6(6\pi w_1)$	$w_1 \in [0, 1]$ $w_i = 0,$ $i = 2, \dots, n$	non-convex, non-uniform
		$f_2(\mathbf{w}) = g(\mathbf{w}) \left[ 1 - (f_1(\mathbf{w})/g(\mathbf{w}))^2 \right]$		
		$g(\mathbf{w}) = 1 + 9 \left[ \left( \sum_{i=2}^n w_i \right) / (n-1) \right]^{1/4}$		

## References

- [1] Drela, M., *Pros & Cons of Airfoil Optimization*, pp. 363–381.
- [2] Besnard, E., Schmitz, A., Boscher, E., Garcia, N., and Cebeci, T., 1998, “Two-dimensional aircraft high lift system design and optimization,” *36th AIAA Aerospace Sciences Meeting and Exhibit*.
- [3] Vicini, A. and Quagliarella, D., 1999, “Airfoil and Wing Design Through Hybrid Optimization Strategies,” *AIAA Journal*, **37**(5), p. 634–641.
- [4] Elham, A. and van Tooren, M. J., 2014, “Winglet multi-objective shape optimization,” *Aerospace Science and Technology*, **37**, p. 93–109.
- [5] Li, J.-Y., Li, R., Gao, Y., and Huang, J., 2010, “Aerodynamic optimization of wind turbine airfoils using response surface techniques,” *Proceedings of the Institution of Mechanical Engineers, Part A: Journal of Power and Energy*, **224**(6), p. 827–838.
- [6] Ju, Y. P. and Zhang, C. H., 2011, “Multi-point robust design optimization of wind turbine airfoil under geometric uncertainty,” *Proceedings of the Institution of Mechanical Engineers, Part A: Journal of Power and Energy*, **226**(2), p. 245–261.
- [7] Ribeiro, A., Awruch, A., and Gomes, H., 2012, “An airfoil optimization technique for wind turbines,” *Applied Mathematical Modelling*, **36**(10), p. 4898–4907.
- [8] Grasso, F., 2012, “Hybrid Optimization for Wind Turbine Thick Airfoils,” *53rd AIAA/ASME/ASCE/AHS/ASC Structures, Structural Dynamics and Materials Conference<BR>20th AIAA/ASME/AHS Adaptive Structures Conference<BR>14th AIAA*.
- [9] Chehour, A., Younes, R., Ilinca, A., and Perron, J., 2015, “Review of performance optimization techniques applied to wind turbines,” *Applied Energy*, **142**, p. 361–388.
- [10] Ali, Q. S. and Kim, M.-H., 2021, “Design and performance analysis of an air-borne wind turbine for high-altitude energy harvesting,” *Energy*, **230**, p. 120829.
- [11] Sobester, A. and Barrett, T., 2008, “Quest for a Truly Parsimonious Airfoil Parameterization Scheme,” *The 26th Congress of ICAS and 8th AIAA ATIO*.
- [12] Sripadkul, V., Padulo, M., and Guenov, M., 2010, “A Comparison of Airfoil Shape Parameterization Techniques for Early Design Optimization,” *13th AIAA/ISSMO Multidisciplinary Analysis Optimization Conference*, American Institute of Aeronautics and Astronautics, Fort Worth, Texas, doi: [10.2514/6.2010-9050](https://doi.org/10.2514/6.2010-9050).
- [13] Masters, D. A., Taylor, N. J., Rendall, T., Allen, C. B., and Poole, D. J., 2015, “Review of Aerofoil Parameterisation Methods for Aerodynamic Shape Optimisation,” *53rd AIAA Aerospace Sciences Meeting*, American Institute of Aeronautics and Astronautics, Kissimmee, Florida, doi: [10.2514/6.2015-0761](https://doi.org/10.2514/6.2015-0761).
- [14] Chen, W., Fuge, M., and Chazan, J., 2017, “Design Manifolds Capture the Intrinsic Complexity and Dimension of Design Spaces,” *Journal of Mechanical Design*, **139**(5), 051102.
- [15] Moazam Sheikh, H., Shabbir, Z., Ahmed, H., Waseem, M. H., and Sheikh, M. Z., 2017, “Computational fluid dynamics analysis of a modified Savonius rotor and optimization using response surface methodology,” *Wind Engineering*, **41**(5), pp. 285–296.
- [16] Jameson, A., 1988, “Aerodynamic design via control theory,” *Journal of Scientific Computing*, **3**(3), p. 233–260.
- [17] Samareh, J. A., 2001, “Survey of Shape Parameterization Techniques for High-Fidelity Multidisciplinary Shape Optimization,” *AIAA Journal*, **39**(5), p. 877–884.
- [18] Sobieczky, H., 1999, “Parametric Airfoils and Wings,” *Recent Development of Aerodynamic Design Methodologies*, E. H. Hirschel, K. Fujii, W. Haase, B. van Leer, M. A. Leschziner, M. Pandolfi, A. Rizzi, B. Roux, K. Fujii, and G. S. Dulikravich, eds., Vol. 65, Vieweg+Teubner Verlag, Wiesbaden, pp. 71–87.
- [19] Farin, G., 1993, “Chapter 4 - The Bernstein Form of a Bézier Curve,” *Curves and Surfaces for Computer-Aided Geometric Design (Third Edition)*, Third edition ed., G. Farin, ed., Academic Press, Boston, pp. 41–63.
- [20] Rogalsky, T. and Derksen, R. W., 2009, “Bézier-PARSEC parameterization for airfoil optimization,” *Canadian Aeronautics and Space Journal*, **55**(3), pp. 163–174.
- [21] Sanaye, S. and Hassanzadeh, A., 2014, “Multi-objective optimization of airfoil shape for efficiency improvement and noise reduction in small wind turbines,” *Journal of Renewable and Sustainable Energy*, **6**(5), p. 053105.
- [22] Han, X. and Zingg, D. W., 2014, “An adaptive geometry parametrization for aerodynamic shape optimization,” *Optimization and Engineering*, **15**(1), pp. 69–91.
- [23] Schramm, U., Pilkey, W. D., DeVries, R. I., and Zebrowski, M. P., 1995, “Shape design for thin-walled beam cross sections using rational B splines,” *AIAA Journal*, **33**(11), p. 2205–2211.
- [24] Sederberg, T. W. and Parry, S. R., 1986, “Free-form deformation of solid geometric models,” *ACM SIGGRAPH Computer Graphics*, **20**(4), p. 151–160.
- [25] Lamousin, H. and Waggenspack, N., 1994, “NURBS-based free-form deformations,” *IEEE Computer Graphics and Applications*, **14**(6), p. 59–65.
- [26] Wendland, H., 2004, “Scattered Data Approximation,” .
- [27] Buhmann, M. D., 2003, “Radial Basis Functions,” .
- [28] Tang, Y., Long, T., Shi, R., Wu, Y., and Gary Wang, G., 2020, “Sequential Radial Basis Function-Based Optimization Method Using Virtual Sample Generation,” *Journal of Mechanical Design*, **142**(11), 111701.
- [29] J. Toal, D. J., Bressloff, N. W., Keane, A. J., and E. Holden, C. M., 2010, “Geometric Filtration Using Proper Orthogonal Decomposition for Aerodynamic Design Optimization,” *AIAA Journal*, **48**(5), p. 916–928.
- [30] Ghoman, S., Wang, Z., Chen, P., and Kapania, R., 2012, “A POD-based Reduced Order Design Scheme for Shape Optimization of Air Vehicles,” *53rd AIAA/ASME/ASCE/AHS/ASC Structures, Structural Dynamics and Materials Conference<BR>20th AIAA/ASME/AHS Adaptive Structures Conference<BR>14th AIAA*.
- [31] Yonekura, K. and Watanabe, O., 2014, “A Shape Parameterization Method Using

- Principal Component Analysis in Applications to Parametric Shape Optimization," *Journal of Mechanical Design*, **136**(12).
- [32] Kedward, L., Allen, C. B., and Rendall, T., *Generic Modal Design Variables for Aerodynamic Shape Optimisation*.
- [33] Poole, D. J., Allen, C. B., and Rendall, T., *Efficient Aero-Structural Wing Optimization Using Compact Aerofoil Decomposition*.
- [34] Hicks, R. M. and Henne, P. A., 1978, "Wing Design by Numerical Optimization," *Journal of Aircraft*, **15**(7), pp. 407–412.
- [35] Kulfan, B. and Bussioletti, J., 2006, "'Fundamental' Parametric Geometry Representations for Aircraft Component Shapes," *11th AIAA/ISSMO Multidisciplinary Analysis and Optimization Conference*, American Institute of Aeronautics and Astronautics, Portsmouth, Virginia, doi: [10.2514/6.2006-6948](https://doi.org/10.2514/6.2006-6948).
- [36] Akram, M. T. and Kim, M.-H., 2021, "CFD Analysis and Shape Optimization of Airfoils Using Class Shape Transformation and Genetic Algorithm—Part I," *Applied Sciences*, **11**(9), p. 3791.
- [37] Viswanath, A., Forrester, A. I. J., and Keane, A. J., 2011, "Dimension Reduction for Aerodynamic Design Optimization," *AIAA Journal*, **49**(6), p. 1256–1266.
- [38] Viswanath, A., Forrester, A. I. J., and Keane, A. J., 2014, "Constrained Design Optimization Using Generative Topographic Mapping," *AIAA Journal*, **52**(5), p. 1010–1023.
- [39] Cinquegrana, D. and Iuliano, E., 2018, "Investigation of adaptive design variables bounds in dimensionality reduction for aerodynamic shape optimization," *Computers & Fluids*, **174**, p. 89–109.
- [40] Chen, W., Chiu, K., and Fuge, M. D., 2020, "Airfoil Design Parameterization and Optimization Using Bézier Generative Adversarial Networks," *AIAA Journal*, **58**(11), p. 4723–4735.
- [41] Chen, W. and Ahmed, F., 2020, "PaDGAN: Learning to Generate High-Quality Novel Designs," *Journal of Mechanical Design*, **143**(3), 031703.
- [42] Oh, S., Jiang, C.-H., Jiang, C., and Marcus, P. S., 2018, "Finding the optimal shape of the leading-and-trailing car of a high-speed train using design-by-morphing," *Computational Mechanics*, **62**(1), pp. 23–45.
- [43] Sheikh, H. M. and Marcus, P. S., 2019, "Vertical Axis Wind Turbine Design Using Design-by-Morphing and Bayesian Optimization," *APS Division of Fluid Dynamics Meeting Abstracts*, p. Q14.007.
- [44] Sheikh, H. M., Callan, T. A., Hennessy, K. J., and Marcus, P. S., 2022, "Optimization of the Shape of a Hydrokinetic Turbine's Draft Tube and Hub Assembly Using Design-by-Morphing with Bayesian Optimization," [arXiv.org](https://arxiv.org/abs/2204.00000).
- [45] Sheikh, H. M., Callan, T., Hennessy, K., and Marcus, P., 2021, "Shape Optimization Methodology for Fluid Flows Using Mixed Variable Bayesian Optimization and Design-by-Morphing," *APS Division of Fluid Dynamics Meeting Abstracts*, p. A15.004.
- [46] Koroglu, S. M. and Ozkol, I., 2019, "optimization of an Airfoil Characteristics to Minimize the Turn Radius of a Small Unmanned Aerial Vehicle," *2019 IEEE 10th International Conference on Mechanical and Aerospace Engineering (ICMAE)*.
- [47] Selig, M. S., 1996, "UIUC Airfoil Data Site," Last access: Feb 2022, <https://m-selig.ae.illinois.edu/ads.html>
- [48] Masters, D. A., Taylor, N. J., Rendall, T. C., Allen, C. B., and Poole, D. J., 2017, "Geometric comparison of aerofoil shape parameterization methods," *AIAA Journal*, **55**(5), pp. 1575–1589.
- [49] Piotrowski, M. G. and Zingg, D. W., 2022, "Investigation of a Smooth Local Correlation-based Transition Model in a Discrete-Adjoint Aerodynamic Shape Optimization Algorithm," *AIAA SCITECH 2022 Forum*.
- [50] He, X., Li, J., Mader, C. A., Yildirim, A., and Martins, J. R., 2019, "Robust aerodynamic shape optimization—From a circle to an airfoil," *Aerospace Science and Technology*, **87**, p. 48–61.
- [51] Kenway, G. K. W. and Martins, J. R. R. A., 2016, "Multipoint Aerodynamic Shape Optimization Investigations of the Common Research Model Wing," *AIAA Journal*, **54**(1), p. 113–128.
- [52] Drela, M., 1989, "XFOIL: An Analysis and Design System for Low Reynolds Number Airfoils," *Lecture Notes in Engineering*, p. 1–12.
- [53] Ronsten, G., 1992, "Static pressure measurements on a rotating and a non-rotating 2.375 m wind turbine blade. Comparison with 2D calculations," *Journal of Wind Engineering and Industrial Aerodynamics*, **39**(1-3), p. 105–118.
- [54] Gigue're, P. and Selig, M. S., 1998, "New Airfoils for Small Horizontal Axis Wind Turbines," *Journal of Solar Energy Engineering*, **120**(2), p. 108–114.
- [55] Jones, B. R., Crossley, W. A., and Lyrantzis, A. S., 2000, "Aerodynamic and Aeroacoustic Optimization of Rotorcraft Airfoils via a Parallel Genetic Algorithm," *Journal of Aircraft*, **37**(6), p. 1088–1096.
- [56] Mueller, T. J. and DeLaurier, J. D., 2003, "AERODYNAMICS OF SMALL VEHICLES," *Annual Review of Fluid Mechanics*, **35**(1), p. 89–111.
- [57] Johnson, F. T., Tinoco, E. N., and Yu, N. J., 2005, "Thirty years of development and application of CFD at Boeing Commercial Airplanes, Seattle," *Computers & Fluids*, **34**(10), p. 1115–1151.
- [58] Batten, W., Bahaj, A., Molland, A., and Chaplin, J., 2006, "Hydrodynamics of marine current turbines," *Renewable Energy*, **31**(2), p. 249–256.
- [59] Lafountain, C., Cohen, K., and Abdallah, S., 2010, "Use of XFOIL in design of camber-controlled morphing UAVs," *Computer Applications in Engineering Education*, **20**(4), p. 673–680.
- [60] Ramanujam, G. and Ozdemir, H., 2017, "Improving Airfoil Lift Prediction," *35th Wind Energy Symposium*.
- [61] Robert J. McGhee, B. S. W., 1988, "experimental results for the eppler 387 airfoil at low reynolds numbers in the langley low-turbulence pressure tunnel,"
- [62] Selig, M. S., 1995, *Summary of low speed airfoil data. Vol. 1*, Virginia Beach, Va. Soartech Publications.
- [63] Morgado, J., Vizinho, R., Silvestre, M., and Páscoa, J., 2016, "XFOIL vs CFD performance predictions for high lift low Reynolds number airfoils," *Aerospace Science and Technology*, **52**, p. 207–214.
- [64] Ashenafi, Y., Pandita, P., and Ghosh, S., 2022, "Reinforcement Learning-Based Sequential Batch-Sampling for Bayesian Optimal Experimental Design," *Journal of Mechanical Design*, **144**(9), 091705.
- [65] Kaisa, M., 1999, *Nonlinear Multiobjective Optimization*, Vol. 12 of International Series in Operations Research & Management Science, Kluwer Academic Publishers, Boston, USA.
- [66] Gunantara, N., 2018, "A review of multi-objective optimization: Methods and its applications," *Cogent Engineering*, **5**(1), p. 1502242.
- [67] Barron F. H., B. B. E., 1996, "Decision quality using ranked attribute weights," *Management Science*, **42**, p. 1515.
- [68] Das I., D. J. E., 1997, "A closer look at drawbacks of minimizing weighted sums of objectives for Pareto set generation in multi-criteria optimization problems," *Structural Optimization*, **14**, p. 63.
- [69] T. C. C., 2007, "Multi-choice goal programming," *Omega*, **35**, p. 389.
- [70] Ghachi, R. F., Alnahhal, W. I., Abdeljaber, O., Renno, J., Tahidul Haque, A. B. M., Shim, J., and Aref, A., 2020, "Optimization of Viscoelastic Metamaterials for Vibration Attenuation Properties," *International Journal of Applied Mechanics*, **12**(10), p. 2050116.
- [71] Vangelatos, Z., Sheikh, H. M., Marcus, P. S., Grigoropoulos, C. P., Lopez, V. Z., Flamourakis, G., and Farsari, M., 2021, "Strength through defects: A novel Bayesian approach for the optimization of architected materials," *Science Advances*, **7**(41), p. eabk2218.
- [72] Schlieter, T. and Dlugosz, A., 2020, "STRUCTURAL OPTIMIZATION OF AEROFOILS FOR MANY CRITERIA," pp. 448–451, doi: [10.21495/5896-3-448](https://doi.org/10.21495/5896-3-448).
- [73] Xu, B., Li, Z., Zhu, Z., Cai, X., Wang, T., and Zhao, Z., 2021, "The Parametric Modeling and Two-Objective Optimal Design of a Downwind Blade," *Frontiers in Energy Research*, **9**, p. 432.
- [74] Chehouri, A., Younes, R., Ilinca, A., and Perron, J., 2016, "Wind Turbine Design: Multi-Objective Optimization," *Wind Turbines - Design, Control and Applications*.
- [75] Rodrigues, S., Bauer, P., and Bosman, P. A., 2016, "Multi-objective optimization of wind farm layouts – Complexity, constraint handling and scalability," *Renewable and Sustainable Energy Reviews*, **65**, pp. 587–609.
- [76] Wang, X. D., Hirsch, C., Kang, S., and Lator, C., 2011, "Multi-objective optimization of turbomachinery using improved NSGA-II and approximation model," *Computer Methods in Applied Mechanics and Engineering*, **200**(9–12), pp. 883–895.
- [77] Rao, A. R., Scanlan, J. P., and Keane, A. J., 2007, "Applying Multiobjective Cost and Weight Optimization to the Initial Design of Turbine Disks," *Journal of Mechanical Design*, **129**(12), pp. 1303–1310.
- [78] Nguyen, P., 2021, "A review of Hybrid/combined methods for trajectory optimization of flight vehicles," *Journal of Physics: Conference Series*, **1958**(1), p. 012032.
- [79] Gao, H., Zhang, Y., Zhou, X., and Li, D., 2018, "Intelligent methods for the process parameter determination of plastic injection molding," *Frontiers of Mechanical Engineering*, **13**(1), 85 (10 pages).
- [80] Wang, D., Geng, L., Zhao, Y.-J., Yang, Y., Huang, Y., Zhang, Y., and Shen, H.-B., 2019, "Artificial intelligence-based multi-objective optimization protocol for protein structure refinement," *Bioinformatics*, **36**(2), pp. 437–448.
- [81] Li, Y., Wei, K., Yang, W., and Wang, Q., 2020, "Improving wind turbine blade based on multi-objective particle swarm optimization," *Renewable Energy*, **161**, pp. 525–542.
- [82] Franco Correia, V., Moita, J. S., Moleiro, F., and Soares, C. M. M., 2021, "Optimization of Metal-Ceramic Functionally Graded Plates Using the Simulated Annealing Algorithm," *Applied Sciences*, **11**(2).
- [83] Ciardiello, A., Rosso, F., Dell'Olmo, J., Ciancio, V., Ferrero, M., and Salata, F., 2020, "Multi-objective approach to the optimization of shape and envelope in building energy design," *Applied Energy*, **280**, p. 115984.
- [84] Fox, A. D., Corne, D. W., Mayorga Adame, C. G., Polton, J. A., Henry, L.-A., and Roberts, J. M., 2019, "An Efficient Multi-Objective Optimization Method for Use in the Design of Marine Protected Area Networks," *Frontiers in Marine Science*, **6**, p. 17.
- [85] Afshari, H., Hare, W., and Tesfamariam, S., 2019, "Constrained multi-objective optimization algorithms: Review and comparison with application in reinforced concrete structures," *Applied Soft Computing*, **83**, p. 105631.
- [86] Gao, Y., Shi, L., and Yao, P., 2000, "Study on multi-objective genetic algorithm," *Proceedings of the 3rd World Congress on Intelligent Control and Automation (Cat. No.00EX393)*, Vol. 1, pp. 646–650 vol.1, doi: [10.1109/WCICA.2000.860052](https://doi.org/10.1109/WCICA.2000.860052).
- [87] Skinner, S. and Zare-Behtash, H., 2018, "State-of-the-art in aerodynamic shape optimisation methods," *Applied Soft Computing*, **62**, pp. 933–962.
- [88] Rahmad, Y., Robani, M. D., Palar, P. S., and Zuhail, L. R., 2020, "Single- and multi-objective optimization of a low-speed airfoil using genetic algorithm," *Tangerang Selatan, Indonesia*, p. 020005, doi: [10.1063/5.0002610](https://doi.org/10.1063/5.0002610).
- [89] Zhao, K., Gao, Z., and tao Huang, J., 2014, "Robust design of natural laminar flow supercritical airfoil by multi-objective evolution method," *Applied Mathematics and Mechanics*, **35**, pp. 191–202.
- [90] Sheikh, H. M. and Marcus, P. S., 2022, "Bayesian Optimization For Multi-Objective Mixed-Variable Problems," *2201.12767*, [http://arxiv.org/abs/2201.12767](https://arxiv.org/abs/2201.12767)
- [91] Deb, K., Pratap, A., Agarwal, S., and Meyarivan, T., 2002, "A fast and elitist multiobjective genetic algorithm: NSGA-II," *IEEE Transactions on Evolutionary Computation*, **6**(2), pp. 182–197.

- [92] Zitzler, E., Deb, K., and Thiele, L., 2000, "Comparison of Multiobjective Evolutionary Algorithms: Empirical Results," *Evol. Comput.*, **8**(2), p. 173–195.
- [93] Ananda, G. K. and Selig, M. S., 2018, "Design of bird-like airfoils," *2018 AIAA Aerospace Sciences Meeting*, p. 0310.
- [94] Li, X., Yang, K., Bai, J., and Xu, J., 2013, "A method to evaluate the overall performance of the CAS-W1 airfoils for wind turbines," *Journal of Renewable and Sustainable Energy*, **5**(6), p. 063118.
- [95] 2022, "Airfoil database search," Last access: May 2022, <http://airfoiltools.com/>